The International Archives of the Photogrammetry, Remote Sensing and Spatial Information Sciences, Volume XLVIII-1/W6-2025
3rd International Workshop on Evaluation and BENCHmarking of Sensors, Systems and
GEOspatial Data in Photogrammetry and Remote Sensing (GEOBENCH), 20–21 November 2025, Wroclaw, Poland

Quantitative Evaluation of Angular, Range, and Reflectance Influences on Laser scanners Using a High-Precision Linear Rail Test System

Jiangyuan Song, Corinna Harmening

Geodetic Institute, Karlsruhe Institute of Technology, Germany
{jiangyuan.song, corinna.harmening}@kit.edu

Keywords: Laser scanner, Point Cloud, Quality Assurance, Reflectance, Rail Test System

Abstract

Laser scanning technology is widely used for precise 3D spatial data acquisition, but measurement precision is affected by factors such as incidence angle, target reflectivity, and range. This study focuses on the automotive-grade Robosense Airy LiDAR and compares its performance with traditional survey-grade laser scanners. Four representative laser scanners — Robosense Airy, Leica MS60 MultiStation, Leica BLK360, and Z+F IMAGER 5016 — were assessed under controlled laboratory conditions. This study quantitatively evaluates the laser scanner measurement precision using a high-precision linear rail test system. Test targets with calibrated reflectance levels were positioned at varying distances and incidence angles. Results reveal distinct performance characteristics across sensors, with survey-grade scanners demonstrating superior precision compared to automotive-grade LiDAR. Users should select sensors that match their application requirements and understand each instrument's response characteristics to exploit its capabilities for precision.

1. Introduction

Laser scanning has become a fundamental technology for acquiring 3D spatial data in applications such as geospatial surveying (Harmening et al., 2021), robotics (Weiss and Biber, 2011), and autonomous driving (Li and Ibanez-Guzman, 2020). The measurement precision of LiDAR systems is influenced by multiple factors, such as the incidence angle, target reflectivity, and range (Kukko et al., 2008). These parameters affect the intensity return, signal-to-noise ratio, and ultimately the precision of derived point clouds. Previous studies have demonstrated that oblique incidence angles and low-reflectivity surfaces tend to increase range noise and systematic bias, while near-normal incidence and high reflectivity improve measurement stability (Soudarissanane et al., 2009). Additionally, instrumental errors, range-dependent errors, such as beam divergence, and atmospheric effects, have been widely reported as critical contributors to the measurement uncertainty (Schmitz et al., 2019).

Although laser scanners have been widely implemented, fully characterizing the geometric and radiometric factors that affect measurement precision remains challenging. Laboratory experiments enable precise control over variables such as target reflectance, range, and incidence angle, allowing rigorous quantification of their individual and combined impacts on laser scanner precision (Linzer et al., 2020) (AbdelGafar et al., 2025). However, systematic comparisons of different sensor classes under identical conditions remain lacking. To support optimal sensor selection and deployment, there is a need for traceable, quantitative tests that evaluate instrument-specific precision characteristics.

This study develops a systematic laboratory-based approach using a high-precision linear rail positioning system to quantify and compare the precision of four representative laser scanners across varying incidence angles, ranges, and reflectance levels. Four representative instruments spanning different precision classes were evaluated: the automotive-grade LiDAR Robosense Airy, the lightweight terrestrial laser scanner (TLS) Leica BLK360, the survey-grade MultiStation Leica MS60, and the high-end TLS Z+F IMAGER 5016 (cf. Figure 1). Test targets with three calibrated reflectance levels were systematically positioned at multiple distances and incidence angles (cf. Figure 2). Point clouds from each scanner were processed using global least-squares plane fitting to quantify the measurement deviations and assess the influence of each factor.

Figure 1. Tested sensors: (a) Robosense Airy LiDAR, (b) Leica BLK360 TLS, (c) Leica MS60 MultiStation, (d) Z+F IMAGER 5016 TLS.

The results reveal heterogeneous performance across instruments, with pronounced reflectance and range dependence for automotive grade sensors and more stable behaviour for survey grade scanners. These findings highlight the importance of understanding each sensor's response characteristics. Sensor selec-

tion involves trade-offs between cost, environmental constraints, and measurement precision requirements. For applications demanding millimetre-level precision, empirical validation and instrument-specific correction strategies are essential to achieve desired performance.

It should be noted that this study focuses on evaluating measurement precision across different laser scanners, quantifying random measurement deviations. The assessment of overall accuracy, including potential systematic measurement deviations, is beyond the scope of the present investigation.

2. Related Work

Laser scanning measurements, whether conducted in terrestrial or airborne settings, are influenced by a wide range of factors, including instrument design, atmospheric conditions, object surface properties, and scan geometry (Soudarissanane et al., 2011). All these factors can cause random and / or systematic measurement deviations. Therefore, such influences are critical in applications such as land mapping, tunnel surveys, structural health monitoring, and autonomous driving. In practice, however, deviations from ideal conditions often cause degradation. For example, in airborne surveys, large incidence angles reduce return intensity and distort land mapping (Wu et al., 2021). In tunnel environments, long ranges and oblique angles lower point density and increase positional errors (Roca-Pardiñas et al., 2014). In structural health monitoring, scan geometry and surface properties affect measurement reliability (Xu et al., 2018). In autonomous driving, wet or low-reflectivity road surfaces often lead to unstable or missing returns (Choe et al., 2023). Among the various influencing factors, incidence angle, range, and surface reflectivity are the most frequently studied and also the easiest to experimentally control.

The shape of the laser footprint on the target surface changes with the incidence angle, becoming elongated and distorted at oblique angles. The angular incidence effect is evident for all targets, and becomes more pronounced at larger incidence angles; this effect is even stronger for bright (high-reflectivity) targets (Kukko et al., 2008). (Kaasalainen et al., 2011) proposed a calibration scheme for TLS based on external targets, considering both distance and incidence angle, and introduced an empirical correction function to compensate for systematic angular incidence effects. At the same time, the incidence angle also affects the strength of the returned signal. (Zhang et al., 2020) found that increasing the incidence angle reduces the backscattered intensity. They proposed that a laser ratio method based on specific laser wavelengths can be used to mitigate these effects.

Range effects represent another major source of variability. (Jutzi and Gross, 2009) proposed an intensity normalization framework that incorporates distance, incidence angle, and atmospheric attenuation. (Höfle and Pfeifer, 2007) emphasized the need for hybrid model- and data-driven strategies. Empirical evidence supports these approaches. (Wu et al., 2021) showed that distance normalization in airborne LiDAR reduces intensity variance and improves classification accuracy. Nevertheless, several studies reported deviations from the theoretical inverse-square law. Causes include beam divergence, detector nonlinearities, and background illumination (Zhang et al., 2020).

Surface reflectivity interacts with both incidence angle and range. This interaction further amplifies their influence on measurement quality. (Laconte et al., 2019) found that automotive-grade LiDAR shows centimeter-level biases under oblique incidence. Such biases are critical in safety-relevant navigation tasks. (Muralikrishnan, 2021) also reported that deviations in terrestrial scanners increase with both distance and incidence angle. Application studies confirm these interactions. (Roca-Pardiñas et al., 2014) showed that tunnel inspection precision is strongly affected by range and incidence geometry. (Pesci and Teza, 2008) demonstrated that low-reflectivity surfaces amplify noise and bias, especially at oblique angles. Collectively, these

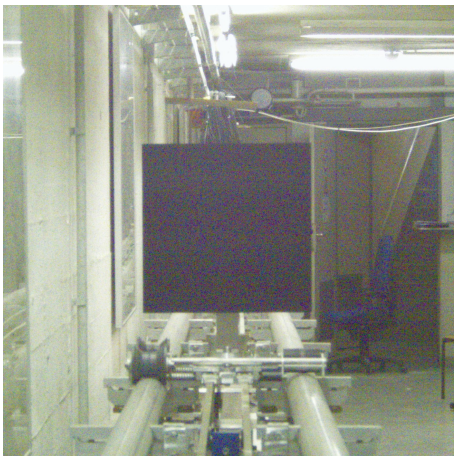

(a) Black Reflectance Target (1.4%)

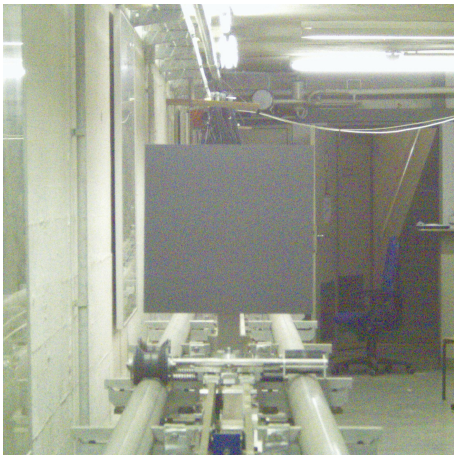

(b) Gray Reflectance Target (10%)

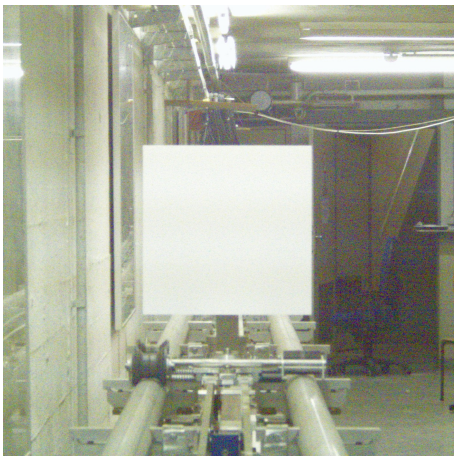

(c) White Reflectance Target (95%)

Figure 2. Reflectance targets (30 cm × 30 cm) used in the experiment: (a) Black (1.4%), (b) Gray (10%), (c) White (95%).

results show that reflectivity and geometric factors jointly determine LiDAR measurement uncertainty across applications.

The above findings also indicate that manufacturer-provided specifications for laser scanners may be insufficient for certain high-precision applications; when possible, users should perform instrument-specific empirical tests. Despite extensive prior work, important gaps remain: systematic comparisons across instrument categories (from automotive LiDARs to survey-grade scanners) are limited, and the combined effects of incidence angle, range, and reflectivity on geometric precision have not been fully quantified. To help address these gaps, we evaluated the precision of the four representative laser scanners under controlled laboratory conditions using 3 distinct reflectance SphereOptics targets.

3. Methodology

This section describes the methodology adopted for evaluating the influences of angular, range, and reflectance variations on LiDAR measurement precision. The following two subsections detail the specifications of the tested laser scanners and the experimental procedure implemented using the high-precision linear rail system (PHIL).

3.1 Laser Scanners

The tested laser scanners are summarized below and are illustrated in Figure 1. For each instrument, both the technical specifications and the data acquisition settings are described in a single item:

- **Robosense Airy LiDAR:** A compact automotive grade LiDAR widely deployed in robotics and now being adopted in indoor surveying instruments. Data was acquired on Ubuntu 22.04 using the official Robosense SDK, with point clouds obtained from the ROS2 `/laserscan` topic and saved in PLY format. Each test captured a single frame (scan frequency: 10 Hz, scan duration: 0.1 s). As a 96-channel LiDAR with channels uniformly distributed across a 180° vertical field of view, point cloud density decreases with increasing range. In practice, approximately four laser point cloud lines intersect the target at 5 m range, two laser point cloud lines at 10 m, and one laser point cloud line at 15 m; notably, no point cloud returns were observed on black targets at 15 m distance.
- **Leica BLK360 TLS:** A lightweight terrestrial laser scanner optimized for rapid 3D data acquisition in architectural and engineering contexts. Only 360-degree scanning is supported; the scan mode was set to "Standard Resolution" (point density: 10 mm at 10 m), with an estimated scan duration of 1 min 50 s.
- **Leica MS60 MultiStation:** A survey-grade total station integrating reflectorless laser scanning, supporting both prism and scanning modes. In scanning mode, the built-in camera was used to select the target area, and the instrument performed single-point scanning via horizontal and vertical motors. The scan resolution was set to 0.1 gon in both directions (15.7 mm at 10 m), with a scan speed of 1000 points per second.
- **Z+F IMAGER 5016 TLS:** A survey-grade terrestrial laser scanner offering high precision and mid-range capabilities for geospatial and industrial measurement tasks. The instrument operates 360-degree scanning; to reduce experimental time, the resolution was set to 25.1 mm at 10 m, with a scan duration of approximately 45 s.

For all four sensors, the acquired point clouds were manually cropped in CloudCompare to isolate the target scan region for subsequent analysis. To ensure consistency in point density across sensors and, consequently, comparability of the precision results, point clouds from the Leica BLK360, Leica MS60, and Z+F IMAGER 5016 were randomly downsampled to 100 points. The Robosense Airy point cloud was not downsampled due to its inherently much lower point density.

3.2 Experimental Procedure

The experimental procedure is illustrated in Figure 3. The experiments were conducted at the Geodetic Institute Karlsruhe using the 24 m high-precision linear rail system PHIL, as shown in Figure 4. The rail system consists of three major parts: A device for installing the instrument to be investigated, a cart that can be automatized moved along the rail track as well as an interferometer, enabling the highly accurate localization of the cart. The rail system can achieve positioning uncertainty of ±0.1 mm and has a maximum velocity of 9 m/s (Hennes, 2006). Since only precision is investigated in this study, the interferometer is currently not used. Test targets comprised three SphereOptics metal panels with calibrated reflectance coatings at 1.4 % (black), 10 % (gray), and 95 % (white) reflectance levels. These targets are subsequently mounted on the cart (see Figure 2).

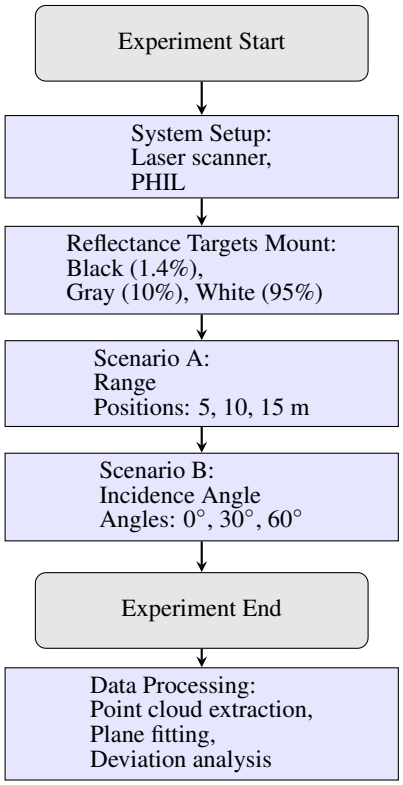

Figure 3. Flowchart of the experimental procedure.

The experimental protocol comprised two main test scenarios, as shown in Flowchart 3. First, for the range and reflectance evaluation (Scenario A), targets were systematically positioned

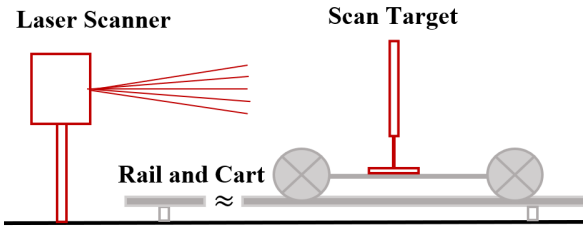

(a) Experiment schematic of PHIL system with laser scanner and targets

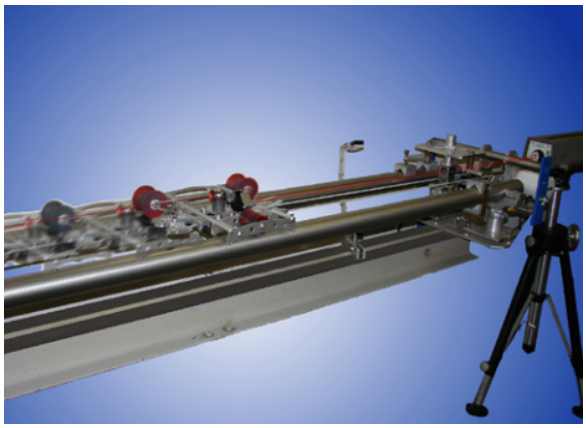

(b) PHIL system at Geodetic Institute Karlsruhe (Hennes, 2006)

Figure 4. High-precision linear rail test system (PHIL): (a) Experiment schematic showing the PHIL system (gray) with laser scanner and scan target (red), (b) PHIL system installation at the Geodetic Institute Karlsruhe

at intervals of 5 m, 10 m, 15 m relative to the scanner to be investigated along the rail. These positions are measured by the motor of the cart (see right side of Figure 4(a)). Second, to investigate the influence of the incidence angle (Scenario B), targets were placed at a fixed distance of 5 m and subsequently rotated to incidence angles of 0°, 30°, and 60° relative to the laser beam axis. Figure 5 shows the connector used to mount the target onto the cart, which allows precise adjustment of the incidence angle via a circular scale.

It is worth noting that some of the investigated distances are in the close range of the used geodetic instruments, which might cause a different behavior than it can be observed for longer distances. These short distances are determined by the maximum range of the automotive LiDAR.

For each configuration, a single scan was performed. For laser scanner point clouds, plane fitting is critical for quantifying random measurement deviations and assessing sensor performance characteristics (Nurunnabi et al., 2014). After the experiments, data processing included point cloud extraction, plane fitting, and deviation analysis, as indicated in the flowchart.

4. Results and Discussion

4.1 Data processing of the results

Data processing was performed in Python, primarily using the Open3D library. Plane fitting was performed on PLY point clouds using a least-squares estimator (Shakarji and Srinivasan, 2013). Each point cloud was read with Open3D and represented as an $N \times 3$ matrix of coordinates. Let $X = \{\mathbf{x}_i\}_{i=1}^{N}$ denote

Figure 5. Connector between the cart and scan target. The bottom circular scale (disc) is used to adjust the incidence angle.

the point set where each $\mathbf{x}_i = (x_i, y_i, z_i)$, and $\bar{\mathbf{x}}$ its centroid. The coordinates were mean-centered:

$$\mathbf{Y}_i = \mathbf{x}_i - \bar{\mathbf{x}} \tag{1}$$

Singular value decomposition (SVD) was applied to the mean-centered coordinate matrix $\mathbf{Y}$ to extract the plane normal. The plane normal vector $\mathbf{n}$ was taken as the right singular vector corresponding to the smallest singular value. To ensure consistent orientation, the normal was flipped if its z-component was negative. The fitted plane equation is expressed as

$$ax+by+cz+d=0, \quad \mathbf{n}=(a,b,c)^{\mathrm{T}}, \quad a^2+b^2+c^2=1 \tag{2}$$

with

$$d = -\mathbf{n} \cdot \bar{\mathbf{x}}. \tag{3}$$

The orthogonal distance from a point $\mathbf{x}_i$ to the fitted plane was computed as

$$d_i = ax_i + by_i + cz_i + d. \tag{4}$$

Point-to-plane distances were summarized by their mean and standard deviation:

$$\bar{d} = \frac{1}{N}\sum_{i=1}^{N} d_i \tag{5}$$

$$s = \sqrt{\frac{1}{N-1}\sum_{i=1}^{N}(d_i - \bar{d})^2}. \tag{6}$$

Figure 6 presents example fits and intensity maps for each sensor at 5 m. The left column shows frontal views of the fitted plane and the right column shows side views; color encodes measured intensity (low to high: blue to red). From the frontal views in Figure 6, the Robosense Airy point cloud clearly shows four distinct line-like bands, a direct consequence of its multi-beam (96-line) scanning architecture. The other sensors produce single-return profiles per scan line but achieve higher apparent point density by rotating the sensor during acquisition. From the side views it is also apparent that the Airy and BLK360 point clouds are visibly thicker and exhibit larger scatter (higher deviations), whereas the MS60 and Z+F 5016 produce much thinner, more tightly clustered point clouds. The next subsection provides a quantitative analysis of these qualitative observations.

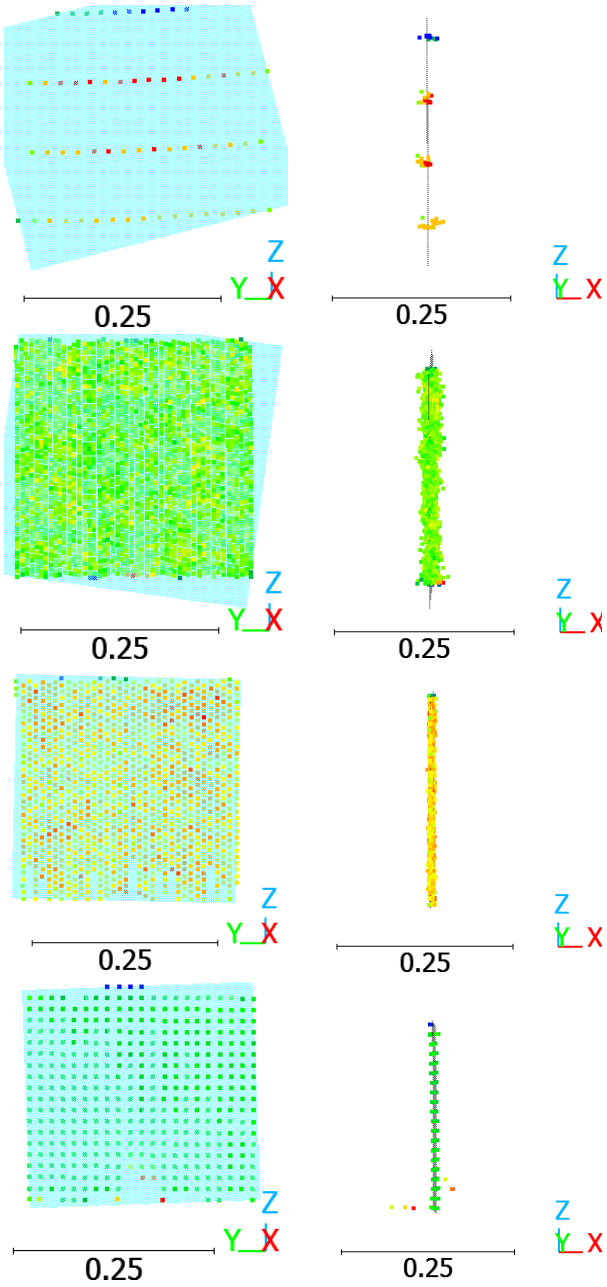

Figure 6. Point cloud plane fitting results for the black target at 5 m for (from top to bottom): (1) Robosense Airy, (2) Leica BLK360, (3) Leica MS60, (4) Z+F IMAGER 5016. Left: front view; right: side view. The blue plane is the fitted surface, and point colors indicate reflectance intensity (blue→green→yellow→red for increasing intensity).

4.2 Analysis of the results

Following data processing, we analyzed the mean and standard deviation of point-to-plane distances. The mean values across all configurations were on the order of 10^{-12} mm, indicating negligible systematic bias. Consequently, standard deviation was adopted as the primary metric for assessing measurement precision. Figures 7 present a comprehensive analysis of point-to-plane standard deviations across all test configurations. Each figure displays results for all four sensors, with the left subplot illustrating distance effects (incidence angle fixed at 0°) and the right subplot showing angular effects (distance fixed at 5 m). Colored lines distinguish the three reflectance targets (black, gray, white). Due to substantial differences in measurement precision across sensors, individual y-axis scales were adopted for each sensor to facilitate visual interpretation. The observed ranges are approximately: Robosense Airy point-to-plane standard deviation spans 8–33 mm; Leica BLK-360 point-to-plane standard deviation ranges 1–7 mm; Leica MS60 point-to-plane standard deviation spans 0.4–1.6 mm; Z+F IMAGER 5016 point-to-plane standard deviation ranges 0.2–1.5 mm (posterior to edge-point filtering). These quantitative differences underscore the substantial disparities in measurement stability between automotive-grade and survey-grade instruments. The experimental design (5–15 m range, 30 cm targets) accommodates Robosense Airy constraints but may not represent optimal conditions for other larger range scanners. Detailed sensor specific analysis follows.

The Robosense Airy LiDAR exhibits strong reflectance dependence, as shown in Figure 7 (first row). Measurement precision degrades significantly at 5 m on higher reflectance targets, with the point-to-plane standard deviation reaching approximately 32 mm on white surfaces. Optimal performance occurs at approximately 10 m range, where fewer laser lines intersect the target and the reflected signal reduced because of the distance, potentially reducing saturation effects. At 15 m, no returns were observed on black targets. Notably, the standard deviation decrease with the increasing incidence angle at 5 m. This reflectance-dependent degradation may be attributed to saturation effects in the single-photon avalanche diode (SPAD) detection principle employed by the Airy (Piron and Redouté, 2024).

The Leica BLK360 TLS demonstrates substantially superior performance compared to the Robosense Airy LiDAR across most configurations, with results comparable but slightly inferior to the MS60 and Z+F systems, as shown in Figure 7 (second row). Point-to-plane standard deviations for the BLK360 range approximately from 1 mm to 7 mm across varying distance and incidence angle combinations. Optimal performance is achieved at approximately 10 m range. Across reflectance types, the BLK360 exhibits markedly superior performance on white targets and degraded performance on black targets. Notably, on white surfaces, the standard deviation increases systematically with the incidence angle, following the expected trend. However, this angular dependence is not clearly observable on black and gray targets. Given its compact form factor and cost-effectiveness, the BLK360 demonstrates reliable performance for centimetre-level precision measurement tasks and is straightforward to operate.

The Leica MS60 MultiStation achieves one of the lowest and most consistent deviations across all test configurations, as shown in Figure 7 (middle row). Similar to the BLK360, the primary performance driver is reflectance rather than distance or incidence angle. On white targets at normal incidence, the point-to-plane standard deviation is approximately 0.4 mm across distances and angles. On gray and black targets the standard deviation increases to roughly 0.7 mm and 1.5 mm, respectively. These results indicate that the survey-grade MS60 is well-suited for high-precision applications and that knowledge of surface reflectance can help users optimize measurement strategies to achieve the best precision.

As shown in Figure 7 (bottom two rows), the Z+F IMAGER 5016 TLS demonstrates notably different behaviour compared to the Leica-series sensors and the Robosense Airy. Unlike the

other instruments, the Z+F performs optimally on the gray reflectance target, achieving submillimeter precision in this configuration. The Z+F exhibits pronounced edge artifacts in raw point clouds, visible in the side view (bottom right) of Figure 6. Point-to-plane distance standard deviations increase substantially at 15 m distance when edge points are retained. This degradation arises from the increased laser spot size at longer ranges; with a beam divergence of approximately 0.3 mrad, the spot diameter reaches approximately 12 mm at 15 m range, causing range uncertainties at target edges. After removal of edge points (denoted ZF2 in the figures), measurement precision improves significantly, approaching or exceeding that of the MS60 across most configurations. It should be noted that scanner acquisition mode influences reported precision: the Z+F IMAGER 5016 was operated in balanced mode, representing a mid-level compromise between point cloud quality and acquisition time. For phase-based scanners such as the Z+F, careful extraction and filtering of mixed pixels at target boundaries is essential for higher precision measurements.

In summary, the tested sensors exhibit distinct performance characteristics determined by their design architectures. The Leica MS60 MultiStation achieves exceptional measurement stability with sub-millimetre precision across all configurations and is recommended for high-precision applications. The Z+F IMAGER 5016 TLS delivers comparable precision but requires filtering of edge points in the point cloud due to spot size effects at longer ranges; however, its scanning speed substantially exceeds the MS60. The Leica BLK360 provides reliable performance for general surveying tasks, while the Robosense Airy is suitable for applications with lower precision demands such as autonomous driving. Users should select instruments matching their specific application requirements to achieve the desired measurement precision.

5. Conclusions and Outlook

This study systematically evaluated the effects of incidence angle, range, and surface reflectance on measurement precision across four representative laser scanners: Robosense Airy, Leica BLK360, Leica MS60, and Z+F IMAGER 5016. The Robosense Airy exhibits substantially lower precision compared to other sensors, with performance degradation particularly pronounced on high-reflectance targets, which is distinct from the other tested instruments. The Leica BLK360 demonstrates superior performance relative to the Airy but remains below that of survey-grade instruments. Without additional point cloud filtering, the Leica MS60 achieves the best precision across diverse configurations. The Z+F IMAGER 5016 exhibits notable edge artifacts in raw point clouds; however, after removal of edge noise, it achieves superior precision exceeding the MS60. Both Leica sensors demonstrate improved performance with increasing target reflectance, whereas the Z+F performs optimally on gray targets in this experiment. These findings underscore the critical role of instrument-specific characteristics in determining measurement precisions and highlight the necessity of empirical validation for precise applications.

It should be noted that the current experimental design encompasses a limited number of angles and distances, particularly for mid-range laser scanning scenarios. The primary objective of this study was to validate the feasibility and reliability of the reflectance target methodology and linear rail test system. In future work, the experimental protocol will be further refined to include more comprehensive angle and distance

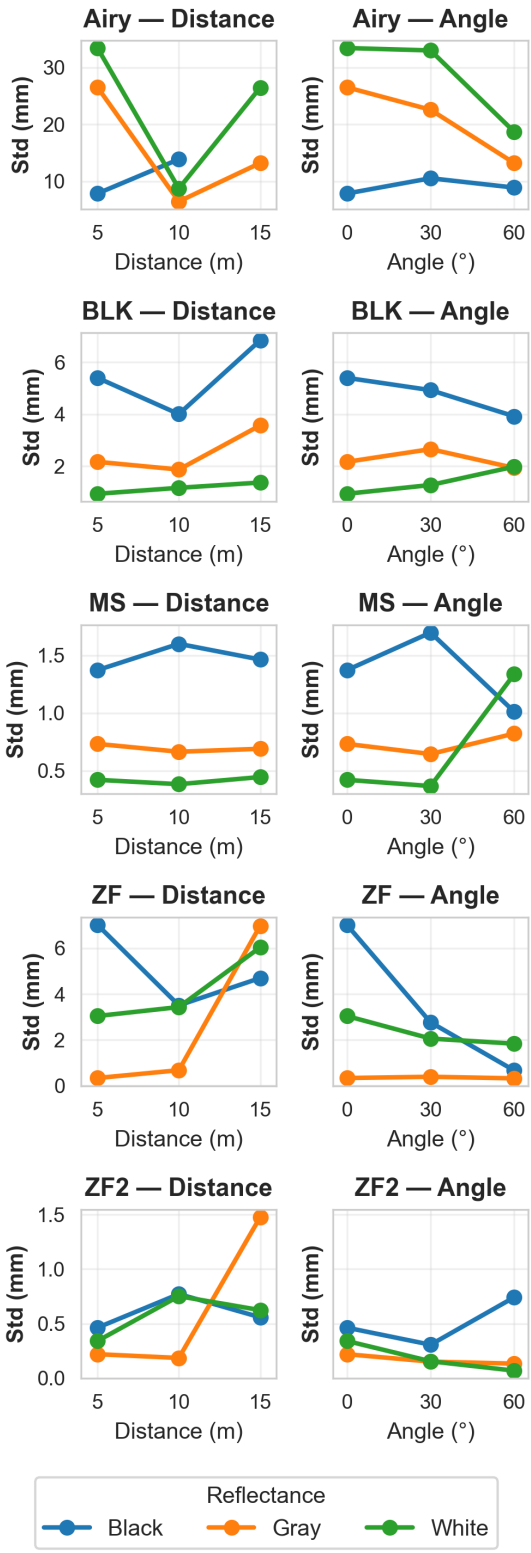

Figure 7. Point-to-plane standard deviations under distance and angle variations (mm). Each row represents a sensor, with the left subplot showing distance impact (angle fixed at 0°) and the right subplot showing angle impact (distance fixed at 5 m). Colored lines represent different reflectance targets (Black, gray, White). ZF2 differs from ZF by removing points with low reflectance or high error at the point cloud on target edges.

https://doi.org/10.5194/isprs-archives-XLVIII-1-W6-2025-219-2025

settings, as well as additional sensor types and reflectance values. Moreover, subsequent experiments will incorporate physical modeling to provide a deeper theoretical explanation of the observed results.

Future work will integrate interferometer measurements with the linear rail system's CAD data to establish ground-truth distance values, enabling rigorous assessment of accuracy and precision. Additionally, the experimental design will be extended to include more sensor types, broader reflectance ranges, and dynamic scenarios.

References

AbdelGafar, O., Palaz, S., Yang, Y., Holst, C., 2025. An efficient strategy for determining intensity-based range variances of terrestrial laser scanners for rigorous deformation analyses. *JISDM 2025*.

Choe, J., Cho, H., Chung, Y., 2023. Performance verification of autonomous driving LiDAR sensors under rainfall conditions in darkroom. *Sensors*, 24(1), 14.

Harmening, C., Hobmaier, C., Neuner, H., 2021. Laser scanner–based deformation analysis using approximating B-spline surfaces. *Remote Sensing*, 13(18), 3551.

Hennes, M., 2006. Präzises und kinematisches Prüfen–Möglichkeiten der Präzisions-High-Speed-Linearmessbahn (PHIL) des Geodätischen Instituts der Universität Karlsruhe. *ZfV-Zeitschrift für Geodäsie, Geoinformation und Landmanagement*.

Höfle, B., Pfeifer, N., 2007. Correction of laser scanning intensity data: Data and model-driven approaches. *ISPRS journal of photogrammetry and remote sensing*, 62(6), 415–433.

Jutzi, B., Gross, H., 2009. Normalization of LiDAR intensity data based on range and surface incidence angle. *Int. Arch. Photogramm. Remote Sens. Spat. Inf. Sci*, 38, 213–218.

Kaasalainen, S., Jaakkola, A., Kaasalainen, M., Krooks, A., Kukko, A., 2011. Analysis of incidence angle and distance effects on terrestrial laser scanner intensity: Search for correction methods. *Remote sensing*, 3(10), 2207–2221.

Kukko, A., Kaasalainen, S., Litkey, P., 2008. Effect of incidence angle on laser scanner intensity and surface data. *Applied Optics*, 47(7), 986–992.

Laconte, J., Deschênes, S.-P., Labussière, M., Pomerleau, F., 2019. Lidar measurement bias estimation via return waveform modelling in a context of 3d mapping. *2019 International Conference on Robotics and Automation (ICRA)*, IEEE, 8100–8106.

Li, Y., Ibanez-Guzman, J., 2020. Lidar for autonomous driving: The principles, challenges, and trends for automotive lidar and perception systems. *IEEE Signal Processing Magazine*, 37(4), 50–61.

Linzer, F., Papčová, M., Neuner, H., 2020. Quantification of systematic distance deviations for scanning total stations using robotic applications. *Contributions to International Conferences on Engineering Surveying: 8th INGEO International Conference on Engineering Surveying and 4th SIG Symposium on Engineering Geodesy*, Springer, 98–108.

Muralikrishnan, B., 2021. Performance evaluation of terrestrial laser scanners—A review. *Measurement Science and Technology*, 32(7), 072001.

Nurunnabi, A., Belton, D., West, G., 2014. Robust statistical approaches for local planar surface fitting in 3D laser scanning data. *ISPRS journal of photogrammetry and Remote Sensing*, 96, 106–122.

Pesci, A., Teza, G., 2008. Effects of surface irregularities on intensity data from laser scanning: an experimental approach. *Annals of Geophysics*, 51(5-6), 839–848.

Piron, F., Redouté, J.-M., 2024. Saturation in spad indirect time-of-flight imagers. *2024 31st IEEE International Conference on Electronics, Circuits and Systems (ICECS)*, IEEE, 1–4.

Roca-Pardiñas, J., Argüelles-Fraga, R., de Asís López, F., Ordóñez, C., 2014. Analysis of the influence of range and angle of incidence of terrestrial laser scanning measurements on tunnel inspection. *Tunnelling and underground space technology*, 43, 133–139.

Schmitz, B., Holst, C., Medic, T., Lichti, D. D., Kuhlmann, H., 2019. How to efficiently determine the range precision of 3D terrestrial laser scanners. *Sensors*, 19(6), 1466.

Shakarji, C. M., Srinivasan, V., 2013. Theory and algorithms for weighted total least-squares fitting of lines, planes, and parallel planes to support tolerancing standards. *Journal of computing and information science in engineering*, 13(3), 031008.

Soudarissanane, S., Lindenbergh, R., Menenti, M., Teunissen, P., 2009. Incidence angle influence on the quality of terrestrial laser scanning points. *ISPRS workshop laserscanning*, ISPRS, 183–188.

Soudarissanane, S., Lindenbergh, R., Menenti, M., Teunissen, P., 2011. Scanning geometry: Influencing factor on the quality of terrestrial laser scanning points. *ISPRS journal of photogrammetry and remote sensing*, 66(4), 389–399.

Weiss, U., Biber, P., 2011. Plant detection and mapping for agricultural robots using a 3D LIDAR sensor. *Robotics and autonomous systems*, 59(5), 265–273.

Wu, Q., Zhong, R., Dong, P., Mo, Y., Jin, Y., 2021. Airborne lidar intensity correction based on a new method for incidence angle correction for improving land-cover classification. *Remote Sensing*, 13(3), 511.

Xu, X., Bureick, J., Yang, H., Neumann, I., 2018. TLS-based composite structure deformation analysis validated with laser tracker. *Composite Structures*, 202, 60–65.

Zhang, C., Gao, S., Li, W., Bi, K., Huang, N., Niu, Z., Sun, G., 2020. Radiometric calibration for incidence angle, range and sub-footprint effects on hyperspectral LiDAR backscatter intensity. *Remote Sensing*, 12(17), 2855.